catalysts

MDPI

Article

Study on the Development of High-Performance P-Mo-V Catalyst and the Influence of Aldehyde Impurities on Catalytic Performance in Selective Oxidation of Methacrolein to Methacrylic Acid

Baohe Wang [1,2], Honggang Dong [1,2], Liang Lu [1,2], Hongxia Liu [1,2], Zhaobang Zhang [1,2] and Jing Zhu [1,2,*]

1 Key Laboratory for Green Chemical Technology of Ministry of Education, R&D Center for Petrochemical Technology, Tianjin University, Tianjin 300072, China; wangbh@tju.edu.cn (B.W.); jesse_hgdong1993@tju.edu.cn (H.D.); lz2019207360@tju.edu.cn (L.L.); liuhongxia0919@tju.edu.cn (H.L.); 2119207004@tju.edu.cn (Z.Z.)

2 Collaborative Innovation Center of Chemical Science and Engineering, Tianjin University, Tianjin 300072, China

* Correspondence: cj_zhu1975@tju.edu.cn; Tel.: +86-22-27406959

Abstract: A series of $K_xH_{1.1-x}Cu_{0.2}Cs_1(NH_4)_{1.5}PVMo_{11}O_{40}$ (KxCuCsNH$_4$PVA) catalysts with different *x* values were synthesized to catalyze the selective oxidation of methacrolein (MAL) to methacrylic acid (MAA). The effects of potassium (K) ions on both the structure and catalytic activity were studied in detail. The optimum $K_{0.6}$CuCsNH$_4$PVA exhibited a large surface area, more acid sites, and abundant active species (V^{4+}/VO^{2+}) in the secondary structure of the Keggin structure, consequently offering good catalytic performance. Furthermore, K ions increased the MAA selectivity at the expense of carbon monoxide and carbon dioxide (together defined as CO_X). Additionally, several process parameters for MAL oxidation were evaluated in the processing experiments. The effects of aldehyde impurities (formaldehyde and propanal) on the catalytic performance were investigated. Possible detrimental effects (catalyst poisoning and structural damage) of aldehyde impurities were excluded. A light decrease in MAL conversion could be attributed to the competitive adsorption of aldehyde impurities and MAL on the catalyst. Hopefully, this work contributes to the design of stable and feasible catalysts for the industrial production of MAA.

Keywords: potassium; methacrolein; formaldehyde; propanal; selective oxidation; methacrylic acid; catalytic performance

Citation: Wang, B.; Dong, H.; Lu, L.; Liu, H.; Zhang, Z.; Zhu, J. Study on the Development of High-Performance P-Mo-V Catalyst and the Influence of Aldehyde Impurities on Catalytic Performance in Selective Oxidation of Methacrolein to Methacrylic Acid. *Catalysts* **2021**, *11*, 394. https://doi.org/10.3390/catal11030394

Academic Editor: Leonarda Francesca Liotta

Received: 19 February 2021
Accepted: 16 March 2021
Published: 19 March 2021

1. Introduction

Methacrylic acid (MAA) is a chemical monomer used for the synthesis of methyl methacrylate (MMA). In addition to the conventional cyanohydrin process for the synthesis of MAA, environmentally friendly routes starting from C_2 or C_4 feedstock are developed. A typical route of the C_2 process is as follows: the hydroformylation of ethylene to propionaldehyde is the first step, then condensation follows with formaldehyde to form methacrolein (MAL), which is then oxidized by oxygen (O_2) to MAA [1–3]. Selective oxidation of MAL to MAA is an important intermediate step in the synthesis of MMA Keggin-type P-Mo-V based on heteropoly acids (HPAs) and their salts are suitable for the selective oxidation of MAL to MAA [4–9]. However, their poor thermal stability and low surface area led to low catalytic activity and high costs of the catalysts. The decomposition of the Keggin structure and irreversible deactivation significantly reduces the lifetime of HPAs catalysts [10–12].

Recently, many attempts have been made to optimize the composition of P-Mo-V catalysts for the selective oxidation of MAL to MAA. Among them, cesium (Cs), ammonium

(NH_4^+), and transition metal ions were introduced into the secondary structure of Keggin-type P-Mo-V catalysts to adjust the texture and redox behaviors, significantly improving the catalytic performance [13–18]. Nonetheless, the modified catalysts have difficulty satisfying the production requirements, and their low selectivity and conversion limit their industrial application. Alkali metals, preferably either cesium or potassium, play an indispensable role in adjusting the acidity and surface area of the catalyst. Several studies on K ions have only focused on the surface morphology [19], thermostability of P-Mo catalysts in acrolein oxidation [20] and insoluble solid phosphotungstate catalysts [21]. Although interesting studies have been conducted, the detailed inherent effect of the K ions on the catalytic activity in the oxidation of MAL to MAA remains unclear.

The MAL feedstock used to produce MAA in the C_2 process often contains aldehyde impurities, such as formaldehyde and propanal. [1–3]. The MAL feedstock containing aldehyde impurities was defined as crude MAL. The crude MAL feedstock obtained from the previous process (hydroxyl aldehyde condensation reaction) requires deep purification to remove the aldehyde impurities. The resulting material was pure MAL. However, the deep purification of MAL would increase the huge operating cost of MAA production. To reduce the complexity of the process and reduce the energy consumption of the equipment, simple separation of the MAL feedstock seems to be feasible. Meanwhile, these impurities were carried into the industrial MAA reactor with crude MAL. In the production of MAA, P-Mo-V catalysts possess the dual properties of high redox activity and strong Brønsted acid. Some possible detrimental effects would occur when aldehyde impurities undergo oxidation and acid catalysis on the catalyst. For instance, Wen et al. found that formaldehyde can rapidly react with hydrocarbons at Brønsted acid sites to form dienes or eventually coke over zeolites and zeotype catalysts [22].

Moreover, some researchers have reported the deactivation of zeolite catalysts in model reactions of propanal [23,24]. In recent years, most studies have been carried out on heteropoly acid catalysts under pure MAL oxidation. Several studies have indicated that there is no catalyst poisoning or deactivation upon a few cycles of pure MAL oxidation. However, these findings are only slightly applicable to a reactor with crude MAL feedstock. Moreover, to our knowledge, little attention has been paid to the possible detrimental effects of aldehyde impurities on P-Mo-V catalysts in the selective oxidation of MAL to MAA. Understanding the possible detrimental effects of formaldehyde and propanal is crucial for the industrial application of catalysts.

In this study, the role of K ions in $K_xH_{1.1-x}Cu_{0.2}Cs_1(NH_4)_{1.5}PVMo_{11}O_{40}$ ($K_xCuCsNH_4PVA$) was studied. Through various characterization methods and accurate experimental data, the optimized catalyst was obtained. Moreover, co-feeding experiments with formaldehyde and propanal were carried out to examine suspected catalyst poisoning or structural damage. To inspect the industrial feasibility of optimized catalysts, a long-term stability test was conducted over the $K_{0.6}CsCuNH_4PVA$ catalyst for 200 h, where the feedstock used is crude MAL. The catalysts exhibited excellent stability and good catalytic performance.

2. Results

2.1. Characterization of Catalysts

2.1.1. Thermogravimetric Analysis

The thermogravimetric analysis (TG) and derivative thermogravimetry (DTG) curves of the uncalcined catalysts at 50–550 °C are shown in Figure 1. All the samples underwent three steps of weightlessness. First, physically adsorbed water and crystal water were lost below 250 °C. The weightlessness ratios of catalyst were as follows: approximately 3.2% for $K_0CuCsNH_4PAV$, 3.5% for $K_{0.6}CuCsNH_4PAV$, and 3.6% for $K_{1.2}CuCsNH_4PAV$. These results indicate that K ions can slightly increase the amount of adsorbed and crystal water. Second, the decomposition of ammonium ions and the elimination of acidic protons start in the 250–430 °C range [25]. The total mass loss was approximately 3.2% for $CuCsNH_4PVA$, 2.7% for $K_{0.6}CuCsNH_4PVA$, and 2.4% for $K_{1.2}CuCsNH_4PVA$. The slight change in the weightlessness ratio was attributed to the elimination of acidic protons due to the release

of the constitution water. All the acidic protons deprive a lattice oxygen and produce constitutional water, leading to the formation of defective Keggin units [26–29]. To illustrate the stability effect of K ions on the Keggin structure, the initial decomposition temperature of this step was calculated using the weightlessness value. The decomposition temperature of $H_4PVMo_{11}O_{40}$ was 250 °C (not shown), which is consistent with previously reported results [16]. The elimination temperature of acidic protons increased with the content of K ions in the series of $K_xCsCuNH_4PVA$ samples [290 °C for $CuCsNH_4PVA$, 310 °C for $K_{0.6}CuCsNH_4PVA$, and 320 °C for $K_{1.2}CuCsNH_4PVA$].

These results indicated that the K ions significantly increased the thermal stability of the catalyst. Notably, the DTG signal of the decomposition of ammonium was centered at approximately 431 °C for $CuCsNH_4PVA$, 420 °C for $K_{0.6}CuCsNH_4PVA$, and 419 °C for $K_{1.2}CuCsNH_4PVA$. It can be inferred that K ions promoted the decomposition of ammonium. In this step, ammonium ions release ammonia gas, leaving behind the corresponding acidic protons. This results in the formation of hydrated protonated heteropolycompounds [16]. The industrial operating temperature is 310 °C, which is lower than 420 °C. Large amounts of ammonium and acidic protons were retained in $K_{0.6}CuCsNH_4PVA$ at this temperature. Finally, the mass gain occurred at approximately 445 °C. This was ascribed to the reoxidation of V^{4+} to V^{5+} during the heating process. No change was observed in the series of $K_xCsCuNH_4PVA$ samples.

From the TG/DTG results, it can be deduced that (1) large amounts of ammonium and acidic protons were retained in $K_{0.6}CuCsNH_4PVA$ at an industrial operating temperature (310 °C); (2) the introduction of K ions significantly increased the thermal stability of the Keggin structure; and (3) K ions facilitated the decomposition of ammonium salt and formed hydrated protonated heteropolycompounds.

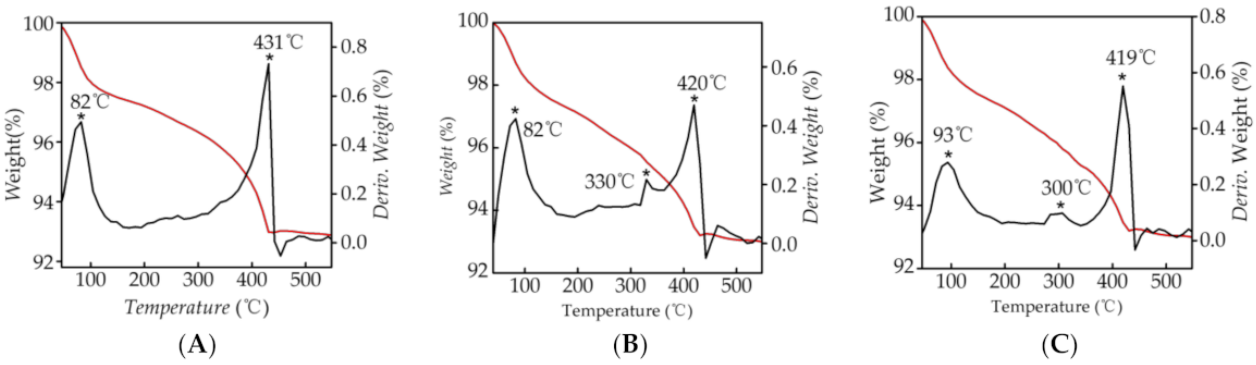

Figure 1. Thermostability of uncalcined samples: (**A**) $K_0CuCsNH_4PAV$; (**B**) $K_{0.6}CuCsNH_4PAV$; (**C**) $K_{1.2}CuCsNH_4PAV$.

2.1.2. Structural Features

The Fourier transform infrared (FT-IR) spectra of the uncalcined and calcined samples are shown in Figure 2. All samples exhibited four Keggin-type characteristic bands at 1064 cm^{-1} (P–O_a), 985 cm^{-1} (Mo–O_d), 897 cm^{-1} (Mo–O_b–Mo) and 798 cm^{-1} (Mo–O_c–Mo) [30]. For uncalcined samples of $K_xCuCsNH_4PAV$, the strong, broad peaks in the range of 3000–3500 cm^{-1} and a peak at 1636 cm^{-1} were observed, which was assigned to the stretching and bending vibrations of –OH in H_2O, respectively. A slight change in this bond indicates K ions can adjust the content of the crystal water. Splitting bonds at 1080 and 997 cm^{-1} were also observed for all the calcined samples, which were assigned to P–O_a and Mo–O_d, respectively. Some previous researches have reported that the substitution of molybdenum (Mo) species in Keggin units by vanadium (V) species decreased oxo-anion symmetry of Keggin units and gave rise to this splitting bond [26]. Interestingly, the splitting bonds disappeared after calcination, and two new bonds at 1039 and 700 cm^{-1} coincidently appeared in calcined samples, which was ascribed to the V–O stretching bands of the vanadium oxide ($V^{5+}O_x$) in the secondary structure [31–33]. The results evidenced that V species were expelled from Keggin units under thermal treatment.

Notably, the vibration intensity of $V^{5+}O_x$ depended on the x value. The relative intensity of this bond strengthened with an increase of potassium content ($x < 0.6$). The results indicated that the introduction of the K ions could promote the expelling of V species into the secondary structure of catalysts. Researchers have shown that VO^{2+} species in the secondary structure are more active than those in the primary structure for MAL oxidation reaction [16,31]. Additionally, Brückner et al. reported that $O_4V^{4+/5+}$=O species connected to Mo^{6+} constituted the active sites for MAL oxidation. The relative intensity of $V^{5+}O_x$ decreased with a further increase of the x value, possibly owing to the significant reduction of acidic protons. Abundant K ions prevented the migration of V species from the Keggin unit. An additional band assigned to molybdenum oxide (MoO_3) at 594 cm^{-1} was observed in the calcined samples [16,31]. Several previous works have shown that the Keggin units partially decompose into low-active MoO_3 during thermal stress [34]. No evidence of an association between potassium ions and MoO_3 was observed in the FT-IR spectra. Moreover, there was a vibrational band at 1406 cm^{-1} for the calcination samples, which was ascribed to NH_4^+ [16]. The results indicate that a large proportion of ammonium remained after calcination.

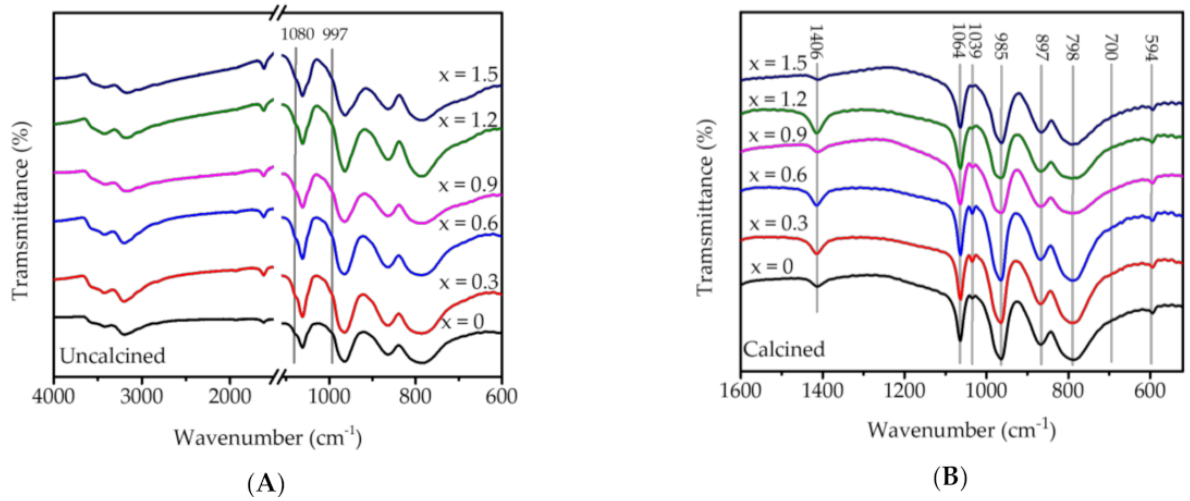

Figure 2. FT-IR spectra of (**A**) uncalcined and (**B**) calcined samples with different x values.

The X-ray diffraction (XRD) patterns of the calcined samples are shown in Figure 3A. The characteristic peaks at 10.7, 26.4, 30.5 and 35.9° were assigned to (110), (222), (400) and (332) planes in the Keggin units for all the samples [16]. Moreover, the diffraction peak of MoO_3 was observed for all the catalysts. The intensity of the peak decreased with the addition of K ions. This indicates that the K ions hindered the decomposition of the Keggin structure into MoO_3 during the thermal treatment. Figure 3 (B) clearly shows that the exact peak positions of catalysts depended on the content of K ions. Taking the peak of the (222) plane as an example, the peak was presented at 26.38° for $CuCsNH_4PAV$, 26.24° for $K_{0.3}CuCsNH_4PAV$, 26.44° for $K_{0.6}CuCsNH_4PAV$, 26.36° for $K_{0.9}CuCsNH_4PAV$, and 26.38° for $K_{1.2}CuCsNH_4PAV$. When K ions were introduced into the catalyst, the release of ammonium was facilitated during calcination, and the secondary structure of the catalyst changed with the redistribution of K ions, ammonium ions and acidic protons. These shifts are related to triclinic crystal unit parameters. The cubic cell parameter α and the crystalline size p were calculated using JADE 6.0 and the Scherrer equation based on the characteristic planes (110), (211), (222), and (400). The results are shown in Table 1. The changes in the cubic cell unit are related to the amount of K ions. $K_{0.6}CuCsNH_4PAV$ reached the optimal balance point, resulting in the smallest cell parameter and crystalline size.

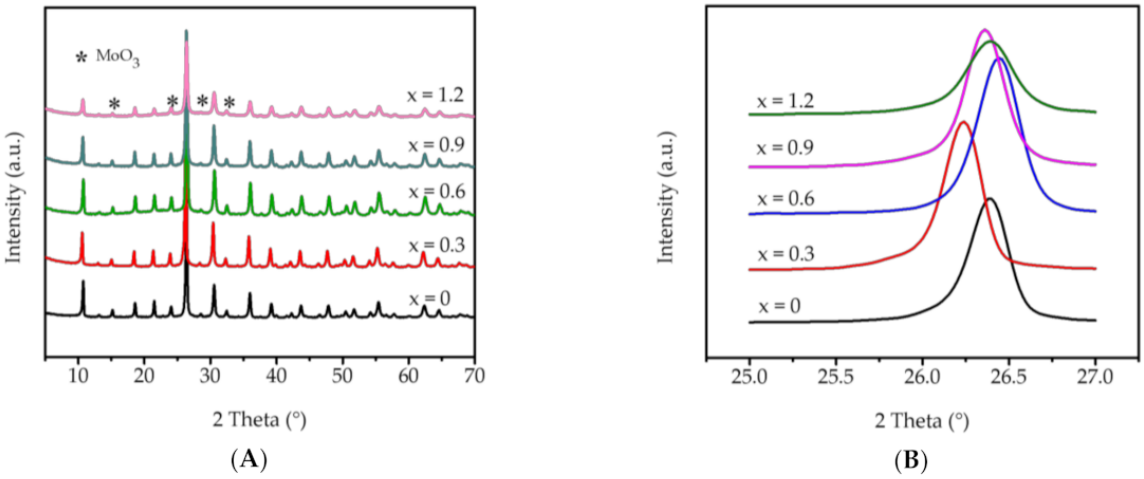

Figure 3. X-ray diffraction spectrogram of (**A**) calcined samples and (**B**) (222) planes of calcined samples.

Table 1. The grain size of $K_xCsCuNH_4PAV$ after calcination.

X Value	Cell Parameter α (nm)	Crystalline Size *p* (nm)
0	1.166	50.3
0.3	1.187	46.2
0.6	1.164	44.8
0.9	1.181	44.6
1.2	1.168	53.7

2.1.3. Morphology Changes with Respect to K Content

The specific surface area, pore volume, and pore diameter of the $K_xCsCuNH_4PAV$ catalysts are shown in Figure 4. The specific surface area of the samples increased when $0 < x < 0.6$, and decreased when $0.6 < x < 1.5$. For $x = 0.6$, the specific surface area was maximized at approximately 29.21 and 15.82 m^2/g for uncalcined and calcined catalysts, respectively. The results indicated that the introduction of K ions ($x < 0.6$) can increase the surface area, but the further addition of K ions ($x > 0.6$) reduces the surface area, owing to the sintering of the catalysts (see below). This phenomenon is related to the aggregation of K ions during calcination. The collapse of the pore structure caused by the elimination of crystal water and the decomposition of ammonium ions during calcination was an important reason for the reduction in the specific surface area.

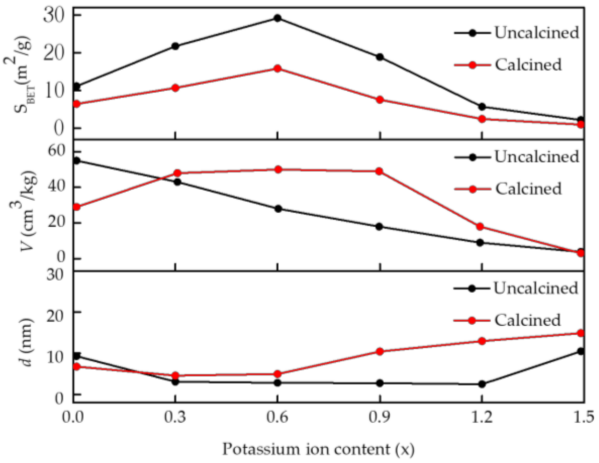

Figure 4. Specific surface area, pore volume and pore diameter of $K_xCsCuNH_4PAV$.

The scanning electron microscopy (SEM) images of the calcined $KxCsCuNH_4PAV$ catalysts are presented in Figure 5a–f. As shown, the particles of the catalyst underwent a gradual process with the x value. The ill-defined particles were observed in the $CuCsNH_4PAV$ catalyst. With the introduction of K ions, the morphology of the catalysts was improved. As shown in Figure 5c, the $K_{0.6}CsCuNH_4PAV$ catalysts exhibited uniform and well-defined porous nanoparticles, which is in favor of desorption of the MAA product. However, further addition of K ions would increase the size of the particles and lead to the sintering of the catalyst. No clear particles were observed in the $K_{1.2}CuCsNH_4PAV$.

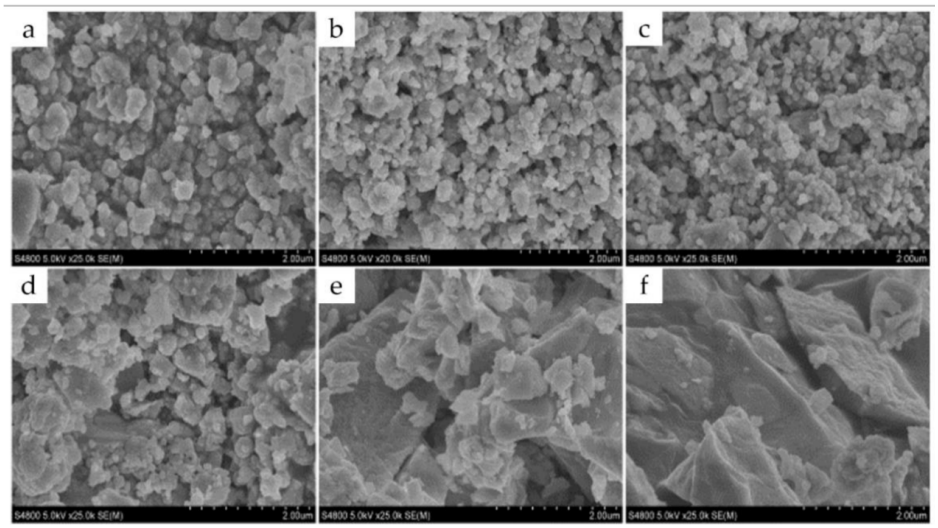

Figure 5. SEM images of the calcined samples: (**a**) $K_0CsCuNH_4PA$; (**b**) $K_{0.3}CsCuNH_4PA$; (**c**) $K_{0.6}CsCuNH_4PA$; (**d**) $K_{0.9}CsCuNH_4PA$; (**e**) $K_{1.2}CsCuNH_4PA$; (**f**) $K_{1.5}CsCuNH_4PAV$.

2.1.4. Effects of K Ions on Intrinsic Properties of Catalysts

The changes in the acidity of catalysts determined by NH_3 temperature-programmed desorption (NH_3-TPD) are shown in Figure 6A. The amount of NH_3 contained not only desorbed from the acid sites but also the release of NH_4^+ during the heating treatment. Corrective treatment was conducted as follows:

$$NH_3^{take\ 2}\left(mmol{\cdot}g^{-1}\right) = NH_3^{take\ 1} - NH_3^{bulk} \quad (1)$$

According to a previous report [26], the peak at <300 °C, 300–450 °C, and >450 °C were ascribed to weak, medium, and strong acid sites, respectively. Compared with $CuCsNH_4PAV$, the shoulder peaks were observed for all the samples, which was ascribed to the ammonia gas released from NH_4^+. This indicates that K ions accelerated the elimination of ammonium, which is consistent with the TG/DTG analysis. Ammonium ions release ammonia gas, leaving behind the corresponding acidic protons. This results in the formation of hydrated protonated heteropolycompounds. Analogous effects were observed in a study on the $(NH_4)_4PMo_{11}FeO_{39}$ catalyst by Knapp et al., and they found that the addition of Fe led to the decomposition of ammonium [15]. According to the NH_3-TPD results, the corrected amount of acid sites increased from 0.42 $mmol{\cdot}g^{-1}$ for $CuCsNH_4PAV$ to 0.59 $mmol{\cdot}g^{-1}$ for $K_{0.3}CuCsNH_4PAV$, and reached the maximum 0.65 $mmol{\cdot}g^{-1}$ for $K_{0.6}CuCsNH_4PAV$. The increase in the number of acid sites is beneficial for MAL oxidation. However, the amount of acid sites in $K_{0.9}CuCsNH_4PAV$ was only 0.31 $mmol{\cdot}g^{-1}$. The decrease in $K_{0.9}CuCsNH_4PAV$ is explained as follows: (a) the substitution of acidic protons by K ions is dominant; (b) excessive K ions reduce the gap between Keggin anions, and the terminal oxygens (Mo=O) prevented NH_3 from contacting the acid sites [35].

H_2 temperature-programmed reduction (H_2-TPR) was used to evaluate the redox properties of the catalysts. The results are shown in Figure 6B. According to the literature [33,36], the reduction peaks of molybdenum and vanadium oxide species were

detected at 500–650 °C for all samples. The reduction peaks of catalysts containing K ions ($0.3 < x < 0.6$) were concentrated at 590 °C, which is lower than the value for $CuCsNH_4PAV$ (600 °C), indicating that the catalysts K by potassium ions were easily reduced.

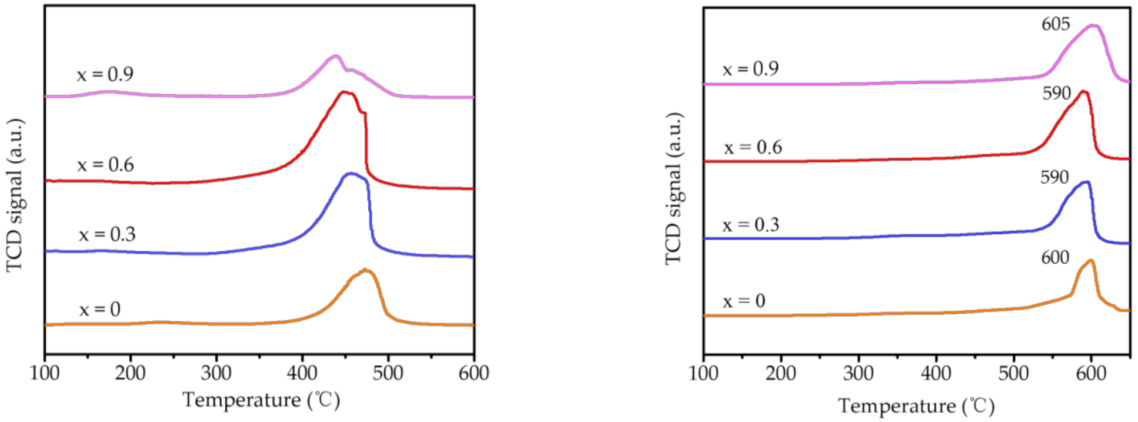

Figure 6. (**A**) NH_3-TPD curves and (**B**) H_2-TPR curves of samples with different x values

The X-ray photoelectron spectroscopy (XPS) results for the valence states of V and Mo are presented in Figure 7. The different valence states of V and Mo species in heteropoly acid catalysts play an important role in the selective oxidation of MAL [37]. Studies have indicated that the V species (V^{4+}/VO^{2+}) are active sites for the selective oxidation of MAL [38–40]. The Mo $3d_{5/2}$ spectra are shown in Figure 7A. Little change was observed in the Mo $3d_{5/2}$ spectra and no Mo^{5+} was found in any of the calcined samples. The results suggested that the chemical state of Mo^{6+} was not affected by K ions. As shown in Figure 7B, two chemical states of V, i.e., V^{5+} (517.7 eV) and V^{4+} (516.5 eV), were observed in the spectra of all the samples [17]. According to the calculation of the corresponding peak, the V^{4+}/V^{5+} ratio increased from 0.22 for $CsCuNH_4PAV$ to 0.31 for $K_{0.6}CuCsNH_4PAV$. The results indicated that the introduction of K ions facilitated the reduction of V^{5+} to V^{4+}. When K^+ met the V^{5+}, the redox reaction was much more likely to occur, whereas the V^{4+}/V^{5+} ratio for $K_{1.2}CuCsNH_4PAV$ was only 0.11. The abundant K^+ counter-ion inhibited the expulsion of V species from the primary structure of Keggin units to the secondary structure. Such phenomena further evidence that the acidic protons played a key role in the expulsion of V species during the calcination process. The abundant active sites (V^{4+}/VO^{2+}) in the catalysts increased the selectivity of MAA.

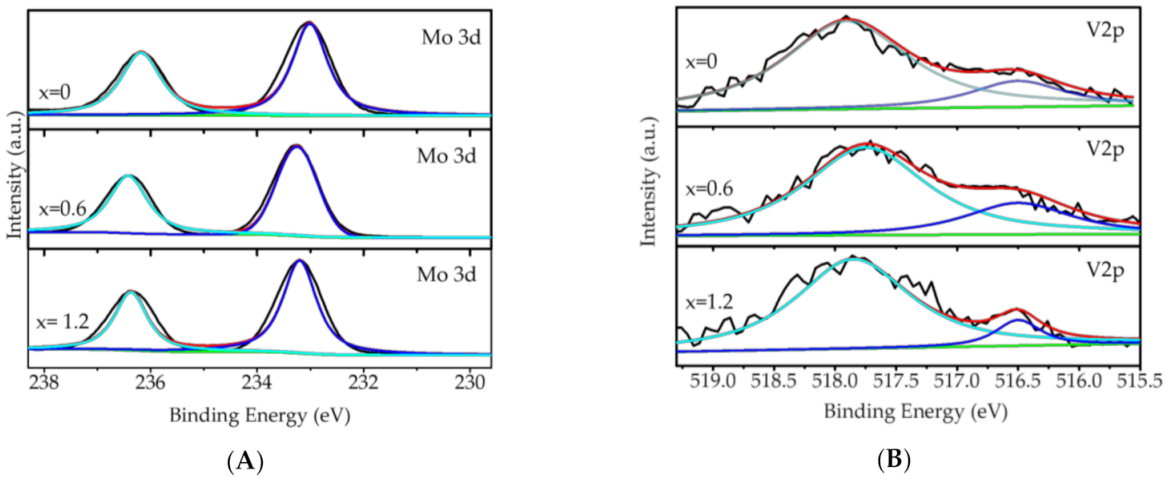

Figure 7. (**A**) Mo 3d and (**B**) V $2p_{3/2}$ spectra of calcined samples.

2.2. Activity of Distinct K Content

P-Mo-V catalysts with Keggin-type structures are composed of $[PVMo_{11}O_{40}]^{4-}$ anions and related cations, which are widely used in various oxidation catalytic reactions [12,41–45]. Among them, the typical application is the selective oxidation of MAL to MAA. In this study, a series of catalysts with different counter-ions were synthesized, e.g., $H_4PVMo_{11}O_{40}$ (HPVA), $Cs_1H_3PVMo_{11}O_{40}$ (CsPVA), $Cs_1(NH_4)_{1.5}H_{1.5}PVMo_{11}O_{40}$ ($CsNH_4PVA$), $Cu_{0.2}Cs_1(NH_4)_{1.5}H_{1.1}PVMo_{11}O_{40}$ ($CuCsNH_4PVA$) and $K_xCu_{0.2}Cs_1(NH_4)_{1.2}H_{1.1-x}PVMo_{11}O_{40}$ ($K_xCuCsNH_4PVA$), to optimize the catalyst composition. To obtain reliable experimental data, the carbon balance was calculated, and it reached 0.99. The samples were collected after 4 h of a stable reaction.

The catalytic performance of the different catalysts is presented in Figure 8A. The results indicated that the presence of cesium, ammonium, copper ions could stabilize the properties of catalysts. The catalytic performance was strongly dependent on counter ions. Moreover, the MAA selectivity in $CuCsNH_4PAV$ cannot satisfy the requirements for industrial production. Therefore, the addition of potassium ions is necessary. The results are shown in Figure 8B. The major by-products of MAL oxidation are acetic acid (AA), carbon monoxide (CO), and carbon dioxide (CO_2). Interestingly, the products distribution was strongly dependent on the K content. The selectivity of MMA increased significantly (from 87% to 93%) for the *x* value from 0 to 0.6. The selectivity of CO_X decreased from 8% to approximately 3%. However, the selectivity of AA was unaffected. The K ions improved the selectivity of MAA at the expense of CO_x. Moreover, the conversion of MAL slightly increased to 83% after introducing K ions.

According to the foregoing characterization results, one of the reasons for the improvement in MAA selectivity was the uniform and well-defined porous nanoparticles after introducing K ions. Another important reason was that K ions boosted the active species (V^{4+}/VO^{2+}) on the surface of the catalyst. No positive effect was observed when additional K ions were introduced. The decrease in MAL conversion may be attributed to the aggregation of K ions blocking the catalyst channel, which prevented MAL from contacting the active sites in the narrow gap between Keggin anions. Based on the above results, $K_{0.6}CuCsNH4PVA$ catalyst with the highest MAA selectivity (93%) and high MAL conversion (83%) was selected for the following research.

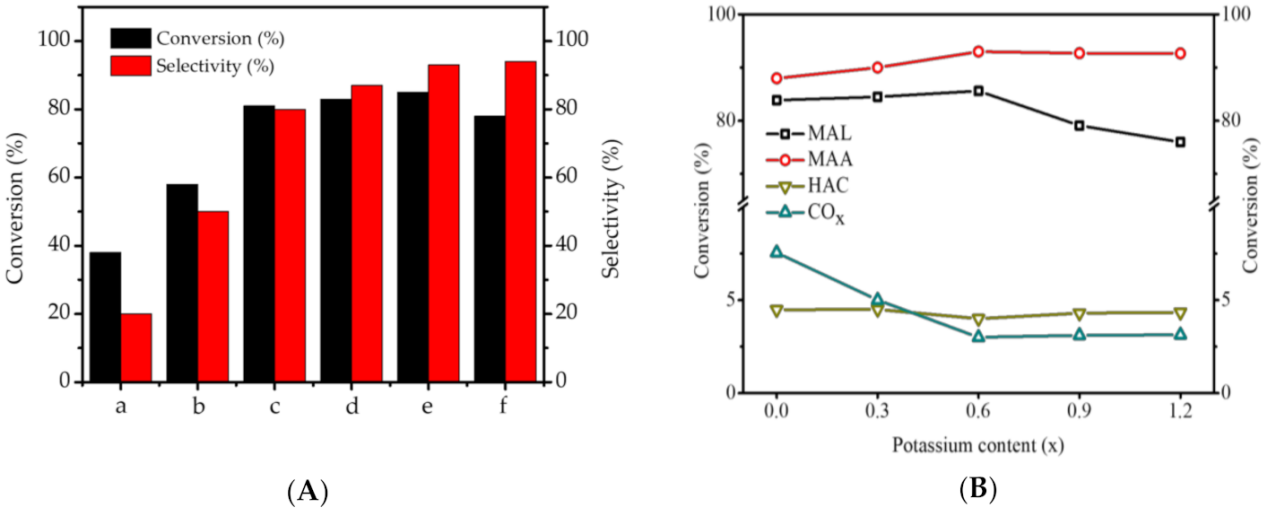

Figure 8. (**A**) Catalytic performance of different catalysts for oxidation MAL to MAA (a: HPVA, b: CsHPVA, c: $CsNH_4PVA$, d: $CuCsNH_4PVA$, e: $K_{0.6}CuCsNH_4PVA$, f: $K_{1.2}CuCsNH_4PVA$). (**B**) Catalytic performance as a function of *x* value in $K_xCuCsNH_4PVA$. Space velocity, 1286 h^{-1}; temperature, 310 °C; reactor inlet composition: 3.3% *v/v* MAL, 9.3% *v/v* O_2, 17.4% *v/v* H_2O and N_2 balance.

2.3. Influence of Temperature and Space Velocity

The plots in Figure 9A show the effect of temperature on catalytic performance in $K_{0.6}CuCsNH_4PVA$. MAL conversion and product distribution are largely dependent on temperature. A low temperature was favorable for the MAA selectivity. The selectivity of CO_x exhibited a greater increase than the selectivity of AA, which provided evidence for the excessive oxidation of AA to produce CO_x. To understand the capacity of catalyst to MAL, the total volumetric flow to volume of catalyst (space velocity) was adjusted from 643 to 2572 h^{-1}. The results are shown in Figure 9B. The distribution of products depends on the space velocity, and a high space velocity is favorable for the MAA selectivity. A low space velocity makes it difficult to maintain the isotherm of the reactor. The large decrease in the selectivity of MAA may be related to the hotspot of the catalyst, where MAA was deeply oxidized and formed by-products. According to the foregoing results, to maximize the yield of desired products, 310 °C and 1286 h^{-1} were selected as appropriate industrial conditions.

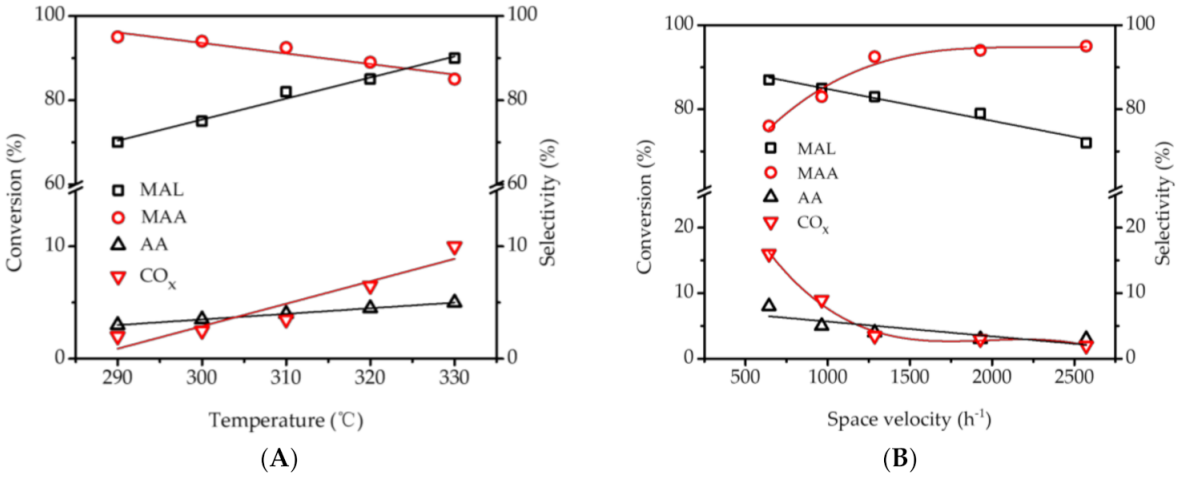

Figure 9. Catalytic performance with respect to the (**A**) temperature and (**B**) space velocity in $K_{0.6}CuCsNH_4PVA$. Reaction pressure, atmospheric pressure; catalyst, 6.001 g, 5 mL; reactor inlet composition: 3.3% *v/v* MAL, 9.3% *v/v* O_2, 17.4% *v/v* H_2O and N_2 balance.

2.4. Influence of Aldehyde Impurities Inlet Concentration

Cofeeding experiments with formaldehyde and propanal were performed on $K_{0.6}CuCsNH_4PAV$ (Figure S1A,B). The conversion of MAL decreased with an increase in the aldehyde impurity content. Interestingly, the selectivity of MAA was almost unaffected. A transient response was carried out to further study the effect of aldehyde impurities on the catalytic performance (Figure 10A). The details are presented in the Supplementary Materials. The change in the conversion of MAL reflects the reversibility of the decay of aldehyde impurities on the catalyst. The results excluded the permanent poisoning of the catalyst caused by formaldehyde and propanal during the selected experimental time.

To further understand the changes in the catalyst structure in the transient response, the reaction was quenched in the middle of another transient response experiment under the same reaction conditions. The catalysts used with runtime were analyzed via FT-IR (Figure S1), XRD (Figure S2), nitrogen adsorption (Table S1) and elemental analysis (Table S1). Small changes were observed in the fresh and spent catalysts under the switch of pure MAL and crude MAL with runtimes. Thus, the large differences in the conversion of MAL in the presence and absence of aldehyde impurities cannot be rationalized by structural changes in the spent catalyst. The reduction in the conversion of MAL is attributed to the competitive adsorption of MAL and aldehyde impurities on the oxidation sites of the catalyst. Additionally, the selected catalyst $K_{0.6}CuCsNH_4PVA$ exhibited good long-term stability (for 200 h) for the oxidation of crude MAL (Figure 10B). Thus, the $K_{0.6}CuCsNH_4PVA$ catalyst can be used for industrial applications.

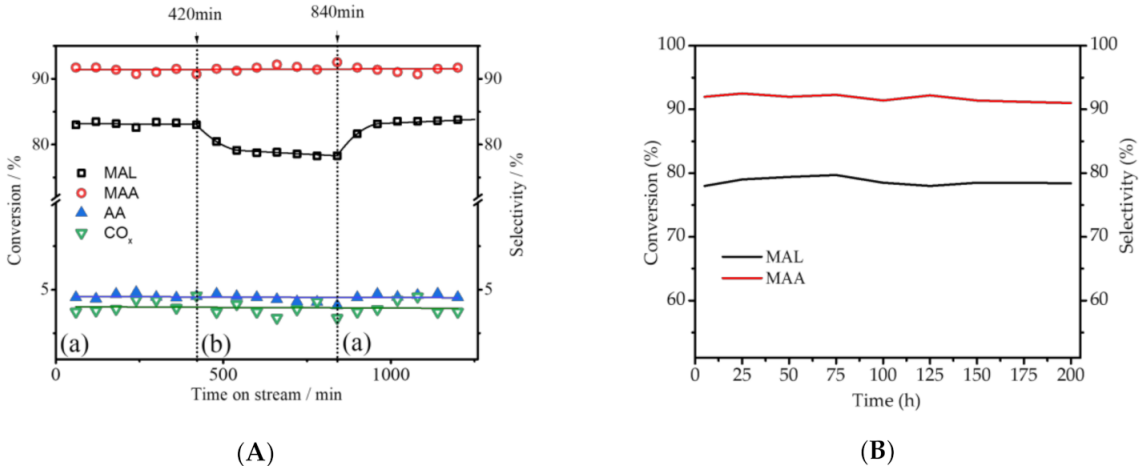

Figure 10. (**A**) Transient response over $K_{0.6}CuCsNH_4PVA$ catalysts with changing the feed from (a) pure MAL to (b) crude MAL at 420 min and subsequently from (b) to (a) at 840 min; (**B**) Long-term performance test with crude MAL for 200 h. Catalysts, $K_{0.6}CuCsNH_4PVA$; Reaction temperature, 310 °C; Space velocity, 1286 h^{-1}, Reaction pressure, atmospheric pressure; Catalyst, 6.001 g, 5 mL; Reactor inlet composition of (a) 3.3% *v/v* MAL, O_2 content 9.3% *v*/*v*, H_2O content 17.4% *v/v* and N_2 balance, and (b) 3.3% *v/v* MAL, 0.06% *v/v* propanal, 0.08% *v/v* formaldehyde; O_2 content 9.3% *v*/*v*, H_2O content 17.4% *v/v* and N_2 balance.

3. Discussion

3.1. Effect of K Ions on P-Mo-V Catalyst

The morphology and structure of the catalyst changed significantly after the introduction of K ions. As indicated by the characterization results, the morphology of catalysts changes from ill-defined particles to clearly visible particles, to uniform particle size and pore structure, finally to the disappearance of pore structure, and even to sintering. These changes directly affected the catalytic performance of the catalyst. Besides, the specific surface area, acid sites and active sites (V^{4+}/VO^{2+}) of the catalyst are also dependent on K ions. The optimized $K_{0.6}CuCsNH_4PVA$ catalyst exhibited a larger surface area of 15.82 m^2/g. It is well known that with a larger surface area, more oxidation sites are available. This is one of the reasons for the improvement of catalytic performance. Acidic protons can activate C–H bonds to form the corresponding oxidized products [46]. As indicated by the NH_4-TPD results, K ions promote the decomposition of ammonium and supplement the catalyst with new acid protons. Acidic protons can easily bind to bridging oxygen (Mo–O–V), resulting in the instability of V–O–Mo bond, which lead to the elimination of lattice oxygen through the release of the constitution water [47,48]. Proton-rich catalysts can easily expel V species under thermal stress. The XPS results indicated that K ions could facilitate the reduction of V^{5+} to V^{4+}. When K^+ met V^{5+}, the redox reaction was much more likely to occur. The presence of abundant active sites (V^{4+}/VO^{2+}) in the catalysts increased the selectivity of MAA. The abundant K^+ counter-ion inhibited the expulsion of V species from the primary structure of Keggin units to the secondary structure.

Notably, the K ions significantly increased the MAA selectivity at the expense of CO_X, which substantially increased the atomic utilization. The reaction over $K_{0.6}CuCsNH_4PAV$ is in accordance with the principle of green chemistry. According to the foregoing analysis, the improvement in the MAA selectivity was also a synergistic effect of multiple factors. First, K ions increased the thermal stability of the Keggin structure during the oxidation reaction. Next, K ions promoted the release of ammonium, forming hydrated protonated heteropolycompounds. The acidic protons can activate the C=O bond and promote the formation of MAA [16]. Third, K ions boosted the active species (V^{4+}/VO^{2+} species) on the catalysts via the excitation of acidic protons. Finally, the uniform and well-defined porous nanoparticles and large surface area promoted the desorption of MAA. To illustrate the effect of K ions on catalytic performance, the Conceptual diagram is shown in Figure 11.

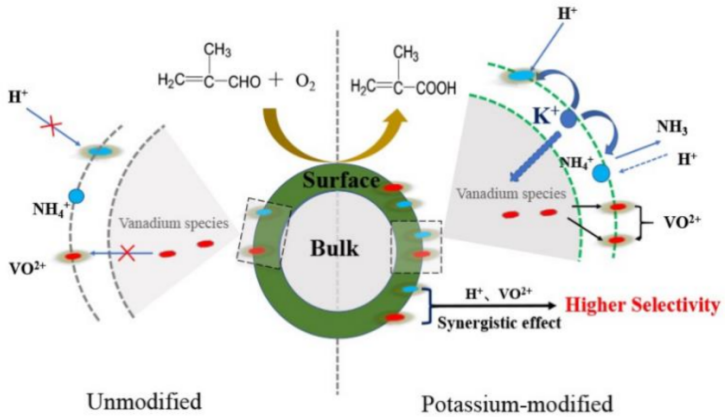

Figure 11. Conceptual diagram of the effects of K ions on P-Mo-V catalyst.

3.2. Effect of Aldehyde Impurities on Catalytic Performance

Aldehyde impurities are carried into the MAA reactor with the MAL feedstock, which may cause catalyst poisoning or irreversible structural damage. Co-feeding experiments with aldehyde impurities were performed. A slight decreased in MAL conversion was found. The reversibility of the MAL conversion in the transient response excluded catalyst poisoning. The characterization of the spent catalysts revealed little structural change under the switch of pure MAL and crude MAL. Moreover, formic acid and propionic acid were detected at the reactor outlet. Aldehyde impurities could not damage the catalyst structure under the selected experimental conditions. The reduction in the conversion of MAL is attributed to the competitive adsorption of MAL and aldehyde impurities on the oxidation sites of the catalyst. Additionally, a long-term stability experiment was conducted within the crude MAL oxidation experiment. The results indicated that the $K_{0.6}CuCsNH_4PAV$ catalyst had good catalytic performance and stability in the oxidation of crude MAL.

4. Conclusions

A series of $KxCuCsNH_4PVA$ catalysts with different counter-ions were synthesized to catalyze the gas-phase oxidation of MAL to MAA. Compared with modified catalysts, the optimum catalyst $K_{0.6}CuCsNH_4PVA$ exhibited a large surface area, more acid sites and, abundant active sites in the secondary structure of the Keggin structure, consequently offering high MAL conversion (83%) and MAA selectivity (93%). Moreover, K ions improved MAA selectivity at the expense of CO_x. Additionally, we performed co-feeding experiments with aldehyde impurities for the first time, and possible detrimental effects of aldehyde impurities on structural damage and poisoning were excluded. A slight decreased in the MAL conversion can be attributed to competitive adsorption of formaldehyde, propanal, and MAL. Long-term stability experiments were performed under the oxidation of crude MAL. The results indicated that the catalyst had long-term stable catalytic performance (for 200 h), and they provide reliable basic data for future applications.

5. Materials and Methods

5.1. Catalyst Preparation

The preparation of precursor heteropoly acids was referred to in the literature [49]. A series of samples were synthesized as follows: MoO_3 and V_2O_5 were dissolved in deionized water. After vigorous stirring at 80 °C for approximately 2 h, 85 wt% H_3PO_4 was dropped into the suspension. The resulting suspension was the precursor solution. The mixture was refluxed and vigorously stirred for approximately 3 h at 92 °C. The solvent was evaporated in a rotary evaporator at 80 °C, and the sample was further dried at 80 °C in an oven for 24 h. A clear yellow powder of HPAV was formed. The fresh catalyst was calcined at 350 °C under an airflow for 12 h. Then, the obtained samples were tableted, crushed, and sieved through a 20-40 mesh screen prior to use. NH_4HCO_3, CsOH, $Cu(CH_3COO)_2$ and KOH were separately dissolved in 5 mL of deionized water and then added dropwise to

the precursor solution with the molar ratio of the target catalyst under stirring at 92 °C for 1 h. The corresponding catalysts can be obtained by repeating the foregoing method. V_2O_5, MoO_3, H_3PO_4, H_3PO_4 and $Cu(CH_3COO)_2$ were purchased from Shanghai Aladdin Biochemical Technology Co., Ltd. (Shanghai, China) NH_4HCO_3, H_3PO_4 and KOH were purchased from Shanghai Macklin Biochemical Co., Ltd.

5.2. Catalyst Characterization

FT-IR were recorded using an FT-IR spectrometer (Nicolet 380, Thermo Electron Corporation, Waltham, MA, USA) with anhydrous KBr as standard. TG analysis was performed using a Shimadzu DTG60H thermogravimetric analyzer (Shimadzu Corporation, Kyoto, Japan). The temperature was programmed to the range of room temperature to 550 min at a heating rate of 5 °C/min. Powder XRD spectroscopy was performed using an X-ray diffractometer (MiniFlex600, Rigaku Corporation, Tokyo, Japan) with Cu-Kα radiation at 40 kV and 200 mA (scanning from 5° to 70° with steps of 0.02°/s and a 2-s acquisition time). The specific surface area and pore structure of the catalyst were tested using an ASAP2460 specific surface area and pore structure analyzer. SEM (SU4800, Hitachi Electronic Electric Appliance Company, Tokyo, Japan) with 5 kV of energy and a 90-mA beam current and transmission electron microscopy (TEM, JEM-2100F, JEOL, Tokyo, Japan) with an acceleration voltage of 200 kV were performed. To identify the acid sites, NH_3-TPD was performed using a Micromeritics AutoChem II 2920 apparatus (Micromeritics Instrument Corporation, Norcross, GA, USA). The redox behavior of the catalysts was determined via temperature-programmed reduction of H_2 with 10% H_2/N_2 (30 mL/min) in the temperature range of 80–650 °C. XPS spectra were obtained using a Kratos Axis Ultra DLD (Manchester, UK) spectrometer with monochromatic Al K radiation.

5.3. Evaluation of Catalyst Activity

Selective oxidation of MAL to MAA was performed using a fixed-bed reactor. The catalyst was loaded into the constant temperature zone of the stainless-steel tubular reactor (10 mm). The catalyst was sandwiched between two layers of quartz wool, and supported by a stainless-steel mesh. MAL and water were transported to the mixer using a micropump. Air and nitrogen were continuously fed into the mixer simultaneously. Experimental parameters are shown in Table 2. The products were analyzed using an Agilent-6820 gas chromatograph (GC) (Agilent Technologies Inc., California, USA) equipped with a thermal conductivity cell detector (TCD) using an HP-INNOWAX capillary column. The off-gas of the oxidation reaction was analyzed using an online GC through an HP-PLOT capillary column.

Table 2. Experimental conditions for the selective oxidation MAL to MAA.

Project	Conditions
MAL content (% v/v)	3.3 [a]
Formaldehyde content (% v/v)	0–0.33
Propanal content (% v/v)	0–0.21
Molar ratio MAL:O_2	1:2.68
H_20 content (% v/v)	17.4 [a]
Total volumetric flow ($L{\cdot}h^{-1}$)	6.43 [a]
Preheater temperature (°C)	130 [a]
Reactor temperature (°C)	280–320
Space velocity (h^{-1})	643–2572
Total pressure (MPa)	atmosphere pressure [a]

[a] Fixed parameters.

MALconversion was defined as follow:

$$\text{MAL conversion (\%)} = 1 - \text{moles of MAL}^{\text{out}}/\text{moles of MAL}^{\text{in}} \times 100, \quad (2)$$

Selectivity to each product was calculated based on carbon basis with the following equations:

$$\text{Selectivity to MAA (\%)} = \text{moles of MAA}^{out}/(\text{moles of MAL}^{in} - \text{moles of MAL}^{out}) \times 100, \quad (3)$$

$$\text{Selectivity to HAC (\%)} = 1/2(\text{moles of HAC}^{out})/(\text{moles of MAL}^{in} - \text{moles of MAL}^{out}) \times 100, \quad (4)$$

$$\text{Selectivity to CO}_x\text{ (\%)} = 1/4(\text{moles of CO}_x{}^{out})/(\text{moles of MAL}^{in} - \text{moles of MAL}^{out}) \times 100, \quad (5)$$

Supplementary Materials: The following are available online at https://www.mdpi.com/2073-4344/11/3/394/s1, Figure S1: The effect of aldehyde impurity on catalytic performance. Figure S2: IR spectra recorded in the transient responses. Figure S3: X-ray diffraction spectrogram recorded in the transient responses. Table S1: Specific surface area and elemental analysis in the transient responses.

Author Contributions: Conceptualization, B.W., J.Z. and H.D.; methodology, B.W. and L.L.; investigation, H.D. and L.L.; writing—original draft preparation, H.D. and L.L; writing—review and editing, H.D. and H.L.; supervision, Z.Z.; project administration, B.W. and J.Z. All authors have read and agreed to the published version of the manuscript.

Funding: This research received no external funding.

Conflicts of Interest: The authors declare no conflict of interest.

References

1. Krill, S.; Offermanns, H.; Rühling, A. Viele Wege führen zum Methacrylsäuremethylester. *Chem. Unserer Zeit.* **2019**, *53*, 148–162. [CrossRef]
2. Zapirtan, V.I.; Mojet, B.L.; Ommen, J.G.V.; Spitzer, J.; Lefferts, L. Gas phase hydroformylation of ethylene using organometalic rh-complexes as heterogeneous catalysts. *Catal. Lett.* **2005**, *101*, 43–47. [CrossRef]
3. Li, Y.C.; Yan, R.Y.; Wang, L.; Liu, L.; Liu, D.; Zhang, H. Synthesis of methacrolein by condensation of propionaldehyde with formaldehyde. *Adv. Mater. Res.* **2012**, *396–398*, 1094–1097. [CrossRef]
4. Marosi, L.; Cox, G.; Tenten, A.; Hibst, H. In Situ XRD Investigations of the $Cs_1H_3PVMo_{11}O_{40}$ Heteropolyacid; Structural Changes Occurring during the Catalytic Methacrolein Oxidation Reaction. *Catal. Lett.* **2000**, *67*, 193–196. [CrossRef]
5. Illies, S.; Kraushaar-Czarnetzki, B. Processing Study on the Stability of Heteropoly Acid Catalyst in the Oxidation of Methacrolein to Methacrylic Acid. *Ind. Eng. Chem. Res.* **2016**, *55*, 8509–8518. [CrossRef]
6. Filimonov, I.N.; Lee, W.H. Methacrylic Acid: Not a Mere Product But Activator in the Catalytic Oxidation of Methacrolein? *Catal. Lett.* **2009**, *131*, 70–75. [CrossRef]
7. Deusser, L.M.; Petzoldt, J.C.; Gaube, J.W.; Hibst, H. Kinetic Model for Methacrolein Oxidation Influence of Cesium and Vanadium on Heteropolyacid Catalysts $Cs_xH_{3-x+y}[PMo_{12-y}V_yO40]$. *Ind. Eng. Chem. Res.* **1998**, *37*, 3230–3236. [CrossRef]
8. Böhnke, H.; Gaube, J.; Petzoldt, J. Selective Oxidation of Methacrolein towards Methacrylic Acid on mixed Oxide (Mo, V, W) Catalysts. Part 1. Studies on Kinetics. *Ind. Eng. Chem. Res.* **2006**, *45*, 8794–8800. [CrossRef]
9. Böhnke, H.; Gaube, J.; Petzoldt, J. Selective Oxidation of Methacrolein towards Methacrylic Acid on Mixed Oxide (Mo, V, W) Catalysts. Part 2. Variation of Catalyst Composition and Comparison with Acrolein Oxidation. *Ind. Eng. Chem. Res.* **2006**, *45*, 8801–8806. [CrossRef]
10. Rocchiccioli-Deltcheff, C.; Aouissi, A.; Bettahar, M.M.; Launay, S.; Fournier, M. Catalysis by 12-Molybdophosphates: 1. Catalytic Reactivity of 12-Molybdophosphoric Acid related to its Thermal Behavior Investigated through IR, Raman, Polarographic, and X-ray Diffraction Studies: A Comparison with 12-Molybdosilicic acid. *J. Catal.* **1996**, *164*, 16–27. [CrossRef]
11. Watzenberger, O.; Emig, G.; Lynch, D.T. Oxydehydrogenation of Isobutyric Acid with Heteropolyacid Catalysts: Experimental Observations of Deactivation. *J. Catal.* **1990**, *124*, 247–258. [CrossRef]
12. Marosi, L.; Arean, C.O. Catalytic Performance of $Cs_x(NH_4)_yH_zPMo_{12}O_{40}$ and related Heteropolyacids in the Methacrolein to Methacrylic Acid Conversion: In situ Structural Study of the Formation and Stability of the Catalytically Active Species. *J. Catal.* **2003**, *213*, 235–240. [CrossRef]
13. Zhang, H.; Yan, R.; Yang, L.; Diao, Y.; Wang, L.; Zhang, S. Investigation of Cu-and Fe-doped $CsH_3PMo_{11}VO_{40}$ Heteropoly Compounds for the Selective Oxidation of Methacrolein to Methacrylic Acid. *Ind. Eng. Chem. Res.* **2013**, *52*, 4484–4490. [CrossRef]
14. Langpape, M.; Millet, J.M.M. Effect of Iron Counter-ions on the Redox Properties of the Keggin-type Molybdophosphoric Heteropolyacid: Part I. An Experimental Study on Isobutane Oxidation Catalysts. *Appl. Catal. A* **2000**, *200*, 89–101. [CrossRef]
15. Knapp, C.; Ui, T.; Nagai, K.; Mizuno, N. Stability of Iron in the Keggin anion of Heteropoly Acid Catalysts for Selective Oxidation of Isobutane. *Catal. Today* **2001**, *71*, 111–119. [CrossRef]
16. Cao, Y.L.; Wang, L.; Zhou, L.L.; Zhang, G.J.; Xu, B.H.; Zhang, S.J. $Cs(NH_4)_xH_{3-x}PMo_{11}VO_{40}$ Catalyzed Selective Oxidation of Methacrolein to Methacrylic Acid: Effects of NH_4^+ on the Structure and Catalytic Activity. *Ind. Eng. Chem. Res.* **2017**, *56*, 653–664. [CrossRef]

17. Zhou, L.; Wang, L.; Diao, Y.; Yan, R.; Zhang, S. Cesium Salts Supported Heteropoly Acid for Oxidation of Methacrolein to Methacrylic acid. *Mol. Catal.* **2017**, *433*, 153–161. [CrossRef]
18. Zhang, H.; Wang, T.; Ma, X.; Zhu, W. Composition, Structural Evolution and the related Property Variations in Preparation of Mixed Cesium/ammonium Acidic salts of Heteropolyacids. *Catalysts* **2016**, *6*, 187. [CrossRef]
19. McMonagle, J.B.; Moffat, J.B. Pore structures of the monovalent salts of the heteropoly compounds, 12-tungstophosphoric and 12-molybdophosphoric acid. *J. Colloid Interface Sci.* **1984**, *2*, 479–488. [CrossRef]
20. Black, J.B.; Clayden, N.J.; Gai, P.L.; Scott, J.D.; Serwicka, E.M.; Goodenough, J.B. Acrolein oxidation over 12-molybdophosphates: I. Characterization of the catalyst. *J. Catal.* **1987**, *106*, 1–15. [CrossRef]
21. Zhao, S.; Xu, G.; Chang, C.; Fang, S.; Liu, Z.; Du, F. Direct conversion of carbohydrates into ethyl levulinate with potassium phosphotungstate as an efficient catalyst. *Catalysts* **2015**, *5*, 1897–1910. [CrossRef]
22. Wen, W.; Yu, S.; Zhou, C.; Ma, H.; Zhou, Z.; Cao, C.; Pan, Y. Formation and Fate of Formaldehyde in Methanol-to-Hydrocarbon Reaction: In Situ Synchrotron Radiation Photoionization Mass Spectrometry Study. *Angew. Chem. Int. Edit.* **2020**, *59*, 4873–4878. [CrossRef] [PubMed]
23. Jun, Y.; Lee, S.; Lee, K.; Choi, M. Effects of secondary mesoporosity and zeolite crystallinity on catalyst deactivation of ZSM-5 in propanal conversion. *Microporous Mesoporous Mat.* **2017**, *245*, 16–23. [CrossRef]
24. Luo, H.; Prasomsri, T.; Román-Leshkov, Y. Al-MFI Nanosheets as Highly Active and Stable Catalysts for the Conversion of Propanal to Hydrocarbons. *Top. Catal.* **2015**, *58*, 529–536. [CrossRef]
25. Liu, S.; Chen, L.; Wang, G.; Liu, J.; Gao, Y.; Li, C.; Shan, H. Effects of Cs-substitution and Partial Reduction on Catalytic Performance of Keggin-type Phosphomolybdic Polyoxometalates for Selective Oxidation of Isobutane. *J. Energy Chem.* **2016**, *25*, 85–92. [CrossRef]
26. Jing, F.; Katryniok, B.; Dumeignil, F.; Bordes-Richard, E.; Paul, S. Catalytic selective oxidation of isobutane to methacrylic acid on supported $(NH_4)_3HPMo_{11}VO_{40}$ catalysts. *J. Catal.* **2014**, *309*, 121–135. [CrossRef]
27. Laronze, N.; Marchal-Roch, C.; Guillou, N.; Liu, F.X.; Herve, G. Solid-state chemistry of ammonium and cesium 1-vanado-11-molybdophosphate and ammonium 12-molybdosilicate: Application to oxidation catalysis. *J. Catal.* **2003**, *220*, 172–181. [CrossRef]
28. Jing, F.; Katryniok, B.; Dumeignil, F.; Bordes-Richard, E.; Paul, S. Catalytic selective oxidation of isobutane over $Cs_x(NH_4)_{3-x}HPMo_{11}VO_{40}$ mixed salts. *Catal. Sci. Technol.* **2014**, *4*, 2938–2945. [CrossRef]
29. Kozhevnikov, I.V. Sustainable heterogeneous acid catalysis by heteropoly acids. *J. Mol. Catal. A Chem.* **2007**, *262*, 86–92. [CrossRef]
30. Sun, M.; Zhang, J.; Cao, C.; Zhang, Q.; Wang, Y.; Wan, H. Significant Effect of Acidity on Catalytic Behaviors of Cs-substituted Polyoxometalates for Oxidative Dehydrogenation of Propane. *Appl. Catal. A* **2008**, *349*, 212–221. [CrossRef]
31. Zhou, L.; Wang, L.; Zhang, S.; Yan, R.; Diao, Y. Effect of Vanadyl Species in Keggin-type Heteropoly Catalysts in Selective Oxidation of Methacrolein to Methacrylic acid. *J. Catal.* **2015**, *329*, 431–440. [CrossRef]
32. Brückner, A.; Scholz, G.; Heidemann, D.; Schneider, M.; Herein, D.; Bentrup, U.; Kant, M. Structural evolution of $H_4PVMo_{11}O_{40}{\cdot}xH_2O$ during Calcination and Isobutane Oxidation: New Insights into Vanadium Sites by a Comprehensive in situ Approach. *J. Catal.* **2007**, *245*, 369–380. [CrossRef]
33. Li, X.K.; Zhao, J.; Ji, W.J.; Zhang, Z.B.; Chen, Y.; Au, C.T.; Han, S.; Hibst, H. Effect of Vanadium Substitution in the Cesium Salts of Keggin-type Heteropolyacids on Propane Partial Oxidation. *J. Catal.* **2006**, *237*, 58–66. [CrossRef]
34. Marosi, L.; Cox, G.; Tenten, A.; Hibst, H. In situ XRD investigations of heteropolyacid catalysts in the methacrolein to methacrylic acid oxidation reaction: Structural changes during the activation/deactivation process. *J. Catal.* **2000**, *194*, 140–145. [CrossRef]
35. Santos, J.S.; Dias, J.A.; Dias, S.C.; Garcia, F.A.; Macedo, J.L.; Sousa, F.S.; Almeida, L.S. Mixed Salts of Cesium and Ammonium Derivatives of 12-tungstophosphoric Acid: Synthesis and Structural Characterization. *Appl. Catal. A Gen.* **2011**, *394*, 138–148. [CrossRef]
36. Damyanova, S.; Spojakina, A.; Jiratova, K. Effect of Mixed Titania-alumina Supports on the Phase Composition of Nimo/TiO_2-Al_2O_3 Catalysts. *Appl. Catal. A Gen.* **1995**, *125*, 257–269. [CrossRef]
37. Marchal-Roch, C.; Julien, C.; Moisan, J.F.; Leclerc-Laronze, N.; Liu, F.X.; Hervé, G. Study of Molybdenyl, Vanadyl and Mixed Ammonium Vanadyl Salts of $[PMo_{12}O_{40}]^{3-}$ as Oxidation Catalysts: Structural Modifications due to Water Vapor. *Appl. Catal. A Gen.* **2004**, *278*, 123–131. [CrossRef]
38. Misono, M.; Nojiri, N. Recent Progress in Catalytic Technology in Japan. *Appl. Catal.* **1990**, *64*, 1–30. [CrossRef]
39. Stytsenko, V.D.; Lee, W.H.; Lee, J.W. Catalyst Design for Methacrolein Oxidation to Methacrylic Acid. *Kinet. Catal.* **2001**, *42*, 212–216. [CrossRef]
40. Chihaia, V.; Sohlberg, K.; Sasca, V.; Doca, N.; Popa, A.; Jaeger, N. Kinetics of the reduction with CO and reoxidation on the 12-molybdophosphoric, 1-Vanado-11-Molybdophosphoric Acids and their Salts with NH_4^+, K^+ and Cs^+ Studied by "in situ" UV–Vis–DRS Spectroscopy. *React. Kinet. Mech. Catal.* **2012**, *105*, 207–221.
41. Lee, J.K.; Melsheimer, J.; Berndt, S.; Mestl, G.; Schlögl, R.; Köhler, K. Transient responses of the local electronic and geometric structures of vanado-molybdo-phoshate catalysts $H_{3+n}PV_nMo_{12-n}O_{40}$ in selective oxidation. *Appl. Catal. A Gen.* **2001**, *214*, 125–148. [CrossRef]
42. Lee, J.K.; Russo, V.; Melsheimer, J.; Köhler, K.; Schlögl, R. Genesis of V^{4+} in heteropoly compounds $Cs_xH_{4-x}PVMo_{11}O_{40}$ during thermal treatment, rehydration and oxidation of methanol studied by EPR spectroscopy. *Phys. Chem. Chem. Phys.* **2000**, *2*, 2977–2983. [CrossRef]

43. Mestl, G.; Ilkenhans, T.; Spielbauer, D.; Dieterle, M.; Timpe, O.; Kröhnert, J.; Schlögl, R. Thermally and chemically induced structural transformations of Keggin-type heteropoly acid catalysts. *Appl. Catal. A Gen.* **2001**, *210*, 13–34. [CrossRef]
44. Ressler, T.; Timpe, O.; Girsdies, F.; Wienhold, J.; Neisius, T. In situ investigations of the bulk structural evolution of vanadium-containing heteropolyoxomolybdate catalysts during thermal activation. *J. Catal.* **2005**, *231*, 279–291. [CrossRef]
45. Jentoft, F.C.; Klokishner, S.; Kröhnert, J.; Melsheimer, J.; Ressler, T.; Timpe, O.; Wienhold, J.; Schlögl, R. The structure of molybdenum-heteropoly acids under conditions of gas-phase selective oxidation catalysis: A multi-method in situ study. *Appl. Catal. A Gen.* **2003**, *256*, 291–317. [CrossRef]
46. Ballarini, N.; Cavani, F.; DeGrand, H.; Etienne, E.; Pigamo, A.; Trifir, F.; Dubois, J.-L. The Oxidation of Isobutane to Methacrylic Acid: An Alternative Technology for MMA Production; Methods and Reagents for Green Chemistry: 2007, 256, New Jersey, USA. In *Methods and Reagents for Green Chemistry*; John Wiley & Sons: Boca Raton, FL, USA, 2007; Volume 256.
47. Misono, M. Unique acid catalysis of heteropoly compounds (heteropolyoxometalates) in the solid state. *Chem. Commun.* **2001**, 1141–1152. [CrossRef]
48. Efremenko, I.; Neumann, R. Computational Insight into the Initial Steps of the Mars-van Krevelen Mechanism: Electron Transfer and Surface Defects in the Reduction of Polyoxometalates. *J. Am. Chem. Soc.* **2012**, *134*, 20669. [CrossRef] [PubMed]
49. Kanno, M.; Yasukawa, T.; Ninomiya, W.; Ooyachi, K.; Kamiya, Y. Catalytic Oxidation of Methacrolein to Methacrylic Acid Over Silica-supported 11-molybdo-1-vanadophosphoric Acid with Different Heteropolyacid loadings. *J. Catal.* **2010**, *273*, 1–8. [CrossRef]